symmetry

IMPACT FACTOR 2.7

CITESCORE 4.9

Article

SND@LHC: A New Experiment in Neutrino Physics at the LHC

Antonia Di Crescenzo and Giuliana Galati

Special Issue

Symmetry and Neutrino Physics: Theory and Experiments

Edited by

Prof. Dr. Antonia Di Crescenzo and Prof. Dr. Giuliana Galati

MDPI

https://doi.org/10.3390/sym15061256

symmetry

MDPI

Article

SND@LHC: A New Experiment in Neutrino Physics at the LHC

Antonia Di Crescenzo [1,*,†] and Giuliana Galati [2,*,†] on behalf of the SND@LHC Collaboration

[1] Università di Napoli Federico II, Istituto Nazionale di Fisica Nucleare, 80126 Napoli, Italy
[2] Università di Bari Aldo Moro, Istituto Nazionale di Fisica Nucleare, 70125 Bari, Italy
* Correspondence: antonia.dicrescenzo@unina.it (A.D.C.); giuliana.galati@uniba.it (G.G.)
† These authors contributed equally to this work.

Abstract: The SND@LHC detector experiment is located at the Large Hadron Collider (LHC), about 480 m downstream of the ATLAS interaction point. The detector is designed to measure, for the first time ever, high-energy neutrinos produced at the LHC in the pseudorapidity region of $7.2 < \eta < 8.4$, which is inaccessible to other LHC experiments. The detector comprises a hybrid system that incorporates multiple components. The detector includes a 830 kg target composed of tungsten plates arranged in alternating layers with nuclear emulsion and electronic trackers: this arrangement functions as an electromagnetic calorimeter. Following the electromagnetic calorimeter, there is a hadronic calorimeter and a muon identification system. The detector possesses the ability to differentiate interactions involving all three neutrino flavours, enabling investigations into the physics of heavy flavour production in the forward region. This research is particularly significant for future circular colliders and high-energy astrophysical neutrino experiments. Furthermore, the detector has the ability to search for the scattering of Feebly Interacting Particles. The detector started operating during the LHC Run 3, and it collected a total of $\sim$39 fb^{-1} in 2022. The detector aims to collect approximately 250 fb^{-1} in the whole of Run 3.

Keywords: neutrino; charm; CERN; LHC

Citation: Di Crescenzo, A.; Galati, G., on behalf of the SND@LHC Collaboration. SND@LHC: A New Experiment in Neutrino Physics at the LHC. *Symmetry* **2023**, *15*, 1256. https:// doi.org/10.3390/sym15061256

Academic Editor: Vladimir Dobrev

Received: 19 March 2023
Revised: 22 April 2023
Accepted: 31 May 2023
Published: 14 June 2023

1. Introduction

The SND@LHC detector is a compact experiment that aims to perform the first observations of neutrinos produced at colliders in an energy range that has never been studied before, exploiting the large number of energetic neutrinos from all flavours produced by the LHC [1,2]. The experiment will study the unexplored pseudorapidity range of $7.2 < \eta < 8.4$, in which a significant portion of neutrinos come from the decay of charmed hadrons [3]: this allows the exploration of heavy flavour production in a region that other LHC experiments cannot access. In addition, SND@LHC exhibits sensitivity towards Feebly Interacting Particles (FIPs), a novel category of particles. FIPs are characterised either by their extremely light mass, and by their infrequent production in collisions involving regular particles, or by extended lifetimes that enable them to travel substantial distances. SND@LHC has the capacity to detect FIPs by observing their scattering of atoms within the detector's target: this direct search approach offers an experimental sensitivity within a region of the FIP mass-coupling parameter space that complements other indirect search methods.

SND@LHC is located about 480 m downstream of the ATLAS interaction point (IP1), in the TI18 tunnel. About 100 m of rock shields the detector from the majority of charged particles generated during collisions in the LHC. The ability to identify charged leptons, and to accurately measure the energy of neutrinos, is of paramount importance for distinguishing between the three neutrino flavours in charged current interactions, and investigating their source. These requirements heavily influenced the design of the SND@LHC apparatus, which also had to consider the spatial limitations imposed by the selected installation site. The installation of SND@LHC took place during Long Shutdown 2, in 2021. The detector started collecting data at the start of LHC Run 3, and it will integrate 250 fb^{-1} until 2025.

2. Materials and Methods

The SND@LHC detector has been designed to identify the three neutrino flavours, measure their energy and conduct a direct search for Feebly Interacting Particles (FIPs). The apparatus comprises three key components: a vertex detector that exhibits a sufficiently high resolution to differentiate the neutrino-interaction vertex from the decay of the τ lepton; a calorimeter capable of measuring both electromagnetic and hadronic energy with a commendable time resolution; and a muon system designed to identify the muon resulting from ν_μ charged-current interactions and the muonic decay of the τ lepton.

Preceding the target region, two planes of scintillator bars are positioned, to serve as a veto for charged particles, predominantly muons originating from IP1. The target region, weighing approximately 830 kg, is equipped with five walls of Emulsion Cloud Chamber (ECC) units, each accompanied by a Scintillating Fibre (SciFi) plane. Each ECC unit comprises emulsion films, which function as high-precision tracking devices, interleaved with passive material that serves as the neutrino target. Tungsten was selected as the passive material, to maximise mass within the given volume. The SciFi planes furnish event timestamps, and offer a suitable time resolution for measuring the time-of-flight of particles originating from IP1. The amalgamation of the emulsion target and the target tracker also serves as an electromagnetic calorimeter, totalling 85 X_0.

The veto system, emulsion target and target tracker are enclosed within a borated polyethylene–acrylic box: this box serves a dual purpose, as a shield against low-energy neutrons, and as a controlled environment for maintaining optimal temperature and humidity conditions for the emulsion films.

The hadronic calorimeter and muon identification system are positioned downstream of the target: they consist of eight iron slabs, collectively spanning 9.5 interaction lengths (λ_{int}), with each slab followed by one or two planes of scintillating bars. The development of the hadronic shower commences within the target region, which contributes an average of 1.5 λ_{int}, resulting in a combined length of approximately 11 λ_{int}: this configuration ensures comprehensive coverage of the hadronic showers. For muon identification, emphasis is placed on the last three planes of scintillator bars: these planes are equipped with double layers of narrower bars, offering increased granularity in both vertical and horizontal directions.

Figure 1 displays the layout of the detector, illustrating all its components, except for the neutron shield. The detector maximises the utilisation of the available space within the TI18 tunnel, to achieve the desired coverage in pseudorapidity. Furthermore, Figure 2 provides both side and top views, showcasing the positioning of the detector within the tunnel.

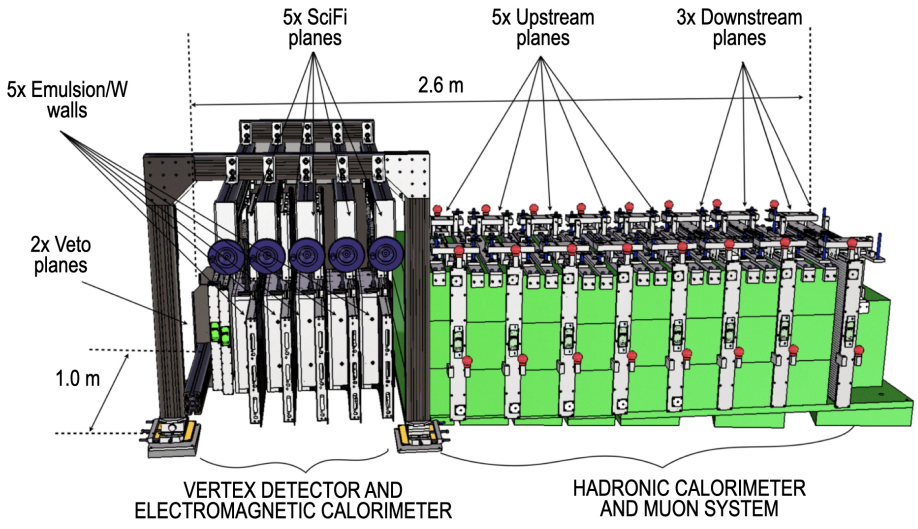

Figure 1. Layout of the SND@LHC experiment [4].

Due to the dimensions of the tunnel, the inclined slope of the floor and the distances of the tunnel walls and floor from the nominal collision axis, the design of the detector faced several constraints. As there was no time available for civil engineering modifications prior to the start of Run 3, the detector layout had to be optimised, to strike a balance between geometric limitations and physics requirements, which included achieving a reliable calorimetric measurement of energy, necessitating approximately 10 λ_{int}, ensuring an efficient muon identification that demanded sufficient material for hadron absorption, and attaining the desired azimuthal angular acceptance with the target region's transverse size. The energy measurement and muon identification constraints imposed a minimum length requirement for the detector, of 2.5 m.

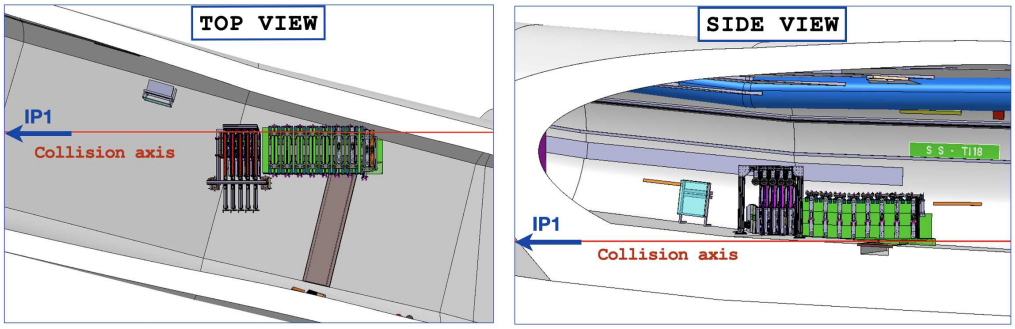

Figure 2. Side and top views of the SND@LHC detector in the TI18 tunnel [4].

3. Physics Goals

Neutrinos serve as a valuable tool for conducting precise tests of the Standard Model (SM) [5–8], and are also instrumental in exploring new physics [9,10]. Figure 3 illustrates the existing measurements of a neutrino cross-section, revealing an unexplored region between 350 GeV and 10 TeV [11]. In the recent decades, investigations into neutrino interactions have primarily focused on low energies. SND@LHC aims to extend these studies to higher energies, reaching up to a few TeV, thereby expanding our understanding of neutrinos in this energy range.

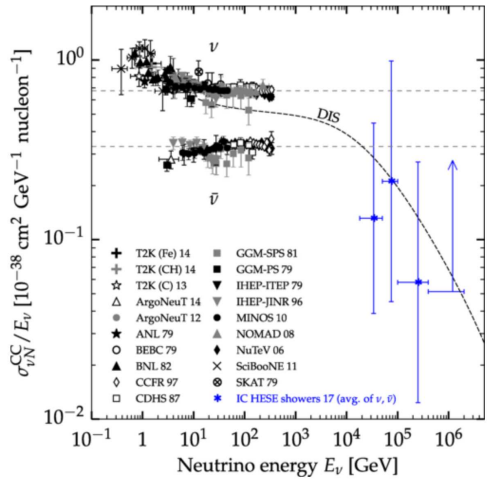

Figure 3. Available measurements of the ν and $\bar{\nu}$ cross-section at different energies [11].

The SND@LHC experiment is driven by multiple objectives, including: studying the production of charmed hadrons in high pseudorapidity pp collisions; testing the lepton flavour universality in neutrino interactions; and measuring the ratio between charged current (CC) and neutral current (NC), to calculate the Weinberg angle as an internal consistency check. Moreover, SND@LHC can perform direct searches for FIPs,

independently of any specific models, by using a recoil signature combined with a time-of-flight measurement, to eliminate neutrino interactions. The experiment's 200 ps time resolution allows it to differentiate between massive FIPs and neutrinos' scattering, by varying degrees of significance, depending on the particle mass [12].

Figure 4 presents the neutrino fluxes as a function of η_ν (pseudorapidity) and E_ν (neutrino energy), within the acceptance range of SND@LHC. The momentum of the two ν_τ produced in the $D_s \to \tau\nu_\tau \to X_\nu^- \tau\nu_\tau$ decay chain led to a correlation between η_ν and E_ν, which can be clearly seen in the right panel. In the case of ν_τ, there was no contamination at low energy. The majority of ν_e and ν_τ originated from the decay of charmed hadrons, with around 10% of ν_e interactions within the acceptance arising from K decay, particularly K_{0s} with energies below 200 GeV. The contribution of beauty hadron decays at IP1 was estimated to be approximately 3%, using the PYTHIA8 [13] event generator. On the other hand, the distributions of ν_μ and $\bar{\nu}_\mu$ were significantly influenced by a softer component resulting from π and K decays, particularly at low energy, which explains the differing intensity scales in Figure 4. The average energies within the acceptance region also differed, with muon neutrinos having an average energy of around 150 GeV, while electron and tau neutrinos had an average energy of approximately 400 GeV.

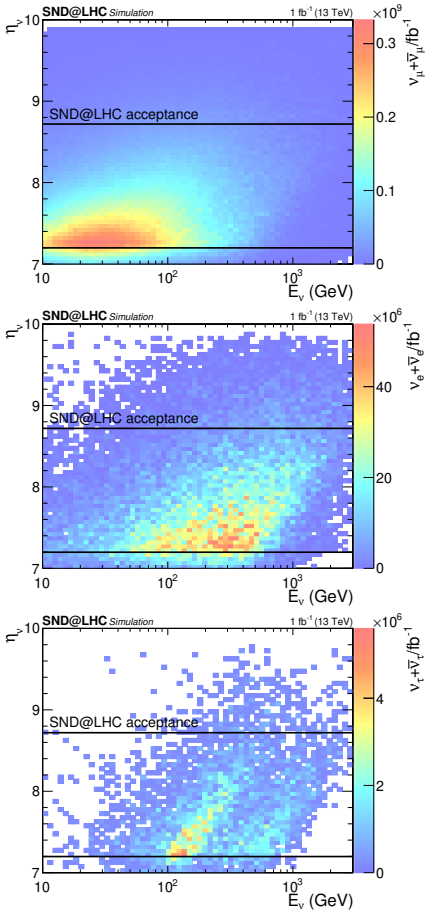

Figure 4. Neutrino and anti−neutrino flux as a function of ν energy E_ν and pseudo-rapidity η_ν for muon (**top**), electron (**middle**) and tau (**bottom**) neutrinos [2].

Figure 5 showcases the energy spectra of neutrinos involved in charged-current deep inelastic scattering (DIS) within the SND acceptance range, specifically in the W target. The displayed spectra are based on extrapolated cross-sections obtained from measured cross-sections of ν_μ and $\bar{\nu}_\mu$ interactions [14], in accordance with the predictions of the Standard Model. For ν_τ interactions, mass effects were taken into account [15], leading to a

reduction in the cross-sections. The data presented in Figure 5 correspond to an integrated luminosity of 250 fb^{-1}.

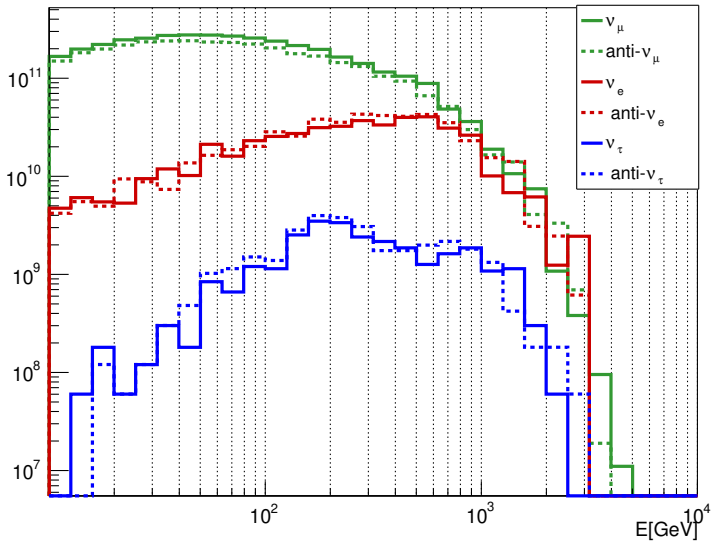

Figure 5. Energy spectrum of the different types of incoming neutrinos and anti-neutrinos, as predicted by the DPMJET [16,17]/FLUKA [18,19] simulation. The result of the simulation has been normalised, to produce neutrino spectra for 250 fb^{-1} [4].

Table 1 provides a summary of the achievable measurements using neutrinos with an integrated luminosity of 250 fb^{-1} at a centre-of-mass energy of 13 TeV. In the search for ν_τ, where the charged lepton is not identified, the main background arises from ν_μ and ν_e charged-current events with charm production, constituting approximately 10% of the total events. By applying straightforward kinematic cuts, this background can be substantially reduced [20], resulting in a final signal-to-background ratio of approximately 4.

Table 1. Measurements proposed by SND@LHC in the analyses of neutrino interactions with Run 3 data [2].

Measurement	**Uncertainty**	
	Stat.	**Sys.**
$pp \to \nu_e X$ cross-section	5%	15%
charmed hadron yield	5%	35%
ν_e/ν_τ ratio for LFU test	30%	22%
ν_e/ν_μ ratio for LFU test	10%	10%
NC/CC ratio	5%	10%

3.1. Charmed Hadron Production at Large η in pp Collisions

Assuming that the Standard Model prediction for the deep inelastic scattering CC cross-section of the electron neutrino is correct, which is supported by results from HERA [21], ν_e can be used to investigate the charm production in the SND@LHC pseudorapidity range: to achieve this, the instrumental effects are unfolded, and the contribution of K is subtracted from the observed energy spectrum of the neutrinos. A method has been developed to estimate the energy spectrum of incoming neutrino flux from the unfolded energy resolution effects: this procedure permits the $pp \to \nu_e X$ cross-section to be measured with a precision of 15%, where the primary source of uncertainty is the systematic uncertainty provided by the unfolding method.

Various event generators predict different levels of K contribution, but they unanimously agree that these events are limited to energies below 200 GeV. Once the K contribution has been subtracted, there remains an additional 20% uncertainty in heavy quark

production, due to the uncertainty in K production. To establish a comprehensive process, a full simulation was implemented, so as to establish a connection between the yield of charmed hadrons in a specific η region and the neutrinos in the corresponding measured η region: this introduced an additional 25% systematic uncertainty into the yield of charmed hadrons. Consequently, the measurement of charmed hadron production in pp collisions can now achieve a statistical uncertainty of around 5%, with the primary source of uncertainty stemming from a systematic error of 35%; moreover, this method can provide valuable information about the gluon parton distribution function in an unexplored x region. As the charmed quark is produced through gluon–gluon scattering, one gluon having $x \sim 2 \times 10^{-1}$, and the other one having $x \sim 2 \times 10^{-6}$, on average, the measurement enables insights into gluon distribution at these specific x values.

3.2. Lepton Flavour Universality Tests in Neutrino Interactions

Cross-section ratios can serve as tests for lepton flavour universality (LFU) in neutrino interactions, by considering two specific ratios: ν_e/ν_τ and ν_e/ν_μ. Tau neutrinos are predominantly produced through the decay $D_s \to \tau\nu_\tau$, with approximately 8% originating from beauty decays. Electron neutrinos arise from decays of D_0, D, D_s and Λ_c. The cross-section ratio $R_{13} = \nu_e/\nu_\tau$ solely relies on charm hadronisation and decay branching fractions. The systematic uncertainty in the fraction of D_s is studied using different event generators, such as PYTHIA8 [13], PYTHIA6 [22] and HERWIG [23], resulting in an uncertainty of 22%: uncertainties related to charm quark production cancel out in this ratio; therefore, R_{13} is sensitive to the ratio of ν-nucleon interaction cross-sections, and allows for LFU testing in neutrino interactions, with a dominant statistical uncertainty of 30%, attributable to the size of the ν_τ sample. The branching fractions in charmed hadron decays for the production of ν_e and ν_μ are nearly equal, effectively cancelling each other out when taking the ratio $R_{12} = N_{\nu_e}/N_{\nu_\mu}$; however, this ratio is significantly impacted by the contamination of ν_μ from decays of π and K, which remains stable above 600 GeV, with an accuracy of 15%. Consequently, the ratio of cross-sections can be expressed as $R_{12} = 1/(1 + \omega_{\pi/K})$, where $\omega_{\pi/K}$ represents the contamination factor.

3.3. Measurement of the NC/CC Ratio

To differentiate between charged-current (CC) and neutral-current (NC) interactions, it is necessary to identify the charged leptons associated with the three flavours. However, in the absence of a magnetic field, distinguishing between CC interactions with neutrinos and anti-neutrinos is not possible, because charge identification is not feasible. Similarly, the flavours of NC interactions cannot be distinguished in a mixed beam. Assuming that the fluxes of ν and $\bar{\nu}$ as a function of neutrino energy are equal, the ratio of NC to CC cross-sections, denoted as R^+, is equal to the ratio of observed events in the respective channels. In the limit of deep inelastic scattering at high momentum transfer, neglecting sea quarks, nuclear effects and QCD effects, R^+ can be expressed as a function of the Weinberg angle [24]:

$$P = \frac{1}{2}\left\{1 - 2\sin^2\theta_W + \frac{20}{9}\sin^4\theta_W - \lambda(1 - 2\sin^2\theta_W)\sin^2\theta_W\right\}. \quad (1)$$

The last term in Equation (1) accounts for the correction related to the non-isoscalar nature of the target, where $\lambda = 0.04$ is the correction factor for tungsten. The uncertainties associated with the measurement are as follows: (a) systematic uncertainties of approximately 10%, which arise from factors such as the asymmetry in the $\nu/\bar{\nu}$ spectra, muon identification, neutron-induced events and CC/NC migration; (b) statistical uncertainties of about 5%, due to the limited number of observed NC interactions. This measurement will serve as a control measurement, to ensure the accuracy and reliability of the data.

3.4. Neutrino-Induced Charm Production

High-energy neutrino interactions are capable of producing charmed hadrons, providing a valuable tool for studying charm physics [8]. Unlike colliding beams, neutrino interactions also involve processes such as quasi-elastic and diffractive scattering, which contribute to the production of charmed hadrons: this unique characteristic makes neutrino interactions particularly suitable for exclusive charm studies. Feynman diagrams depicting the production of charmed hadrons in neutrino and anti-neutrino interactions are shown in Figure 6. Numerous experiments have reported data on charmed hadron production in neutrino and anti-neutrino charged-current interactions. The NuTeV experiment [25], for instance, collected a substantial number of charmed hadron candidates (5102 in ν_μ and 1458 in $\overline{\nu}_\mu$ interactions) within a (x, Q^2) region that overlapped with the region being explored by SND@LHC.

Nuclear emulsion technology offers a unique advantage, in identifying charmed hadrons through the observation of a two-vertex topology, eliminating the need for kinematical cuts. Among the emulsion experiments with the largest neutrino flux, CHORUS [26] measured 2013 charm candidates from ν_μ interactions, and 32 from $\overline{\nu}_\mu$ interactions. The OPERA experiment [27] reported a tau-neutrino candidate with charmed hadron production. However, no charm candidate from electron–neutrino interactions has been reported, thus far.

In contrast to regular neutrino scattering, where the presence of valence quarks favours the d quark as the target, compensating for the Cabibbo angle suppression, charmed hadron production in anti-neutrino interactions predominantly involves the anti-strange quark in the nucleon, as depicted in the right-hand panel of Figure 6. Measurements conducted at SND@LHC can be utilised to determine the s-quark content of the nucleon, providing valuable information for precision tests of the Standard Model.

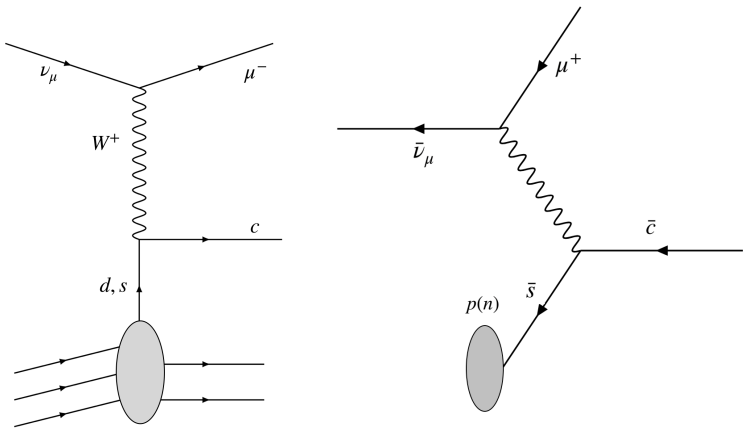

Figure 6. Charm production in neutrino (**a**) and anti-neutrino (**b**) charged-current interactions.

In cases where the lepton produced in a neutrino charged-current interaction cannot be identified, the primary background for searches involving ν_τ comes from interactions of $\nu_\mu(\bar{\nu}_\mu)$ and $\nu_e(\bar{\nu}_e)$ with subsequent charmed hadron production. However, the OPERA experiment [20] has demonstrated that a cut-based analysis can effectively reject such events, by utilising kinematical characteristics. Specifically, the expected back-to-back alignment of the lepton and the hadronic jet in the transverse plane can be exploited as a kinematical feature, to distinguish signal events from background events.

4. Future Prospects

In light of the unique capabilities of the SND@LHC detector in distinguishing all three neutrino flavours, and accurately measuring their energy, an upgrade proposal for the High-Luminosity LHC (HL-LHC) has been put forward [28]. The upgraded version

would involve the use of two detectors. The first detector would be positioned in the same pseudorapidity region as the current SND@LHC detector (see Figure 7, and would focus on measuring charm production and conducting lepton flavour universality tests with neutrinos, at a precision level of 1%. The second detector would be located in the region with $4 < \eta < 5$, and would primarily perform measurements of neutrino cross-sections. This detector would benefit from the overlap with the LHCb experiment, which would help reduce systematic uncertainties. To achieve an increased azimuth angle coverage, the proposal suggests exploring potential locations in existing caverns that are closer to the interaction point: this would allow for better coverage of the neutrino interactions in the desired regions. The second module of the upgraded SND@LHC would serve as a near detector, aimed at reducing systematic uncertainties, and improving the overall precision of the measurements.

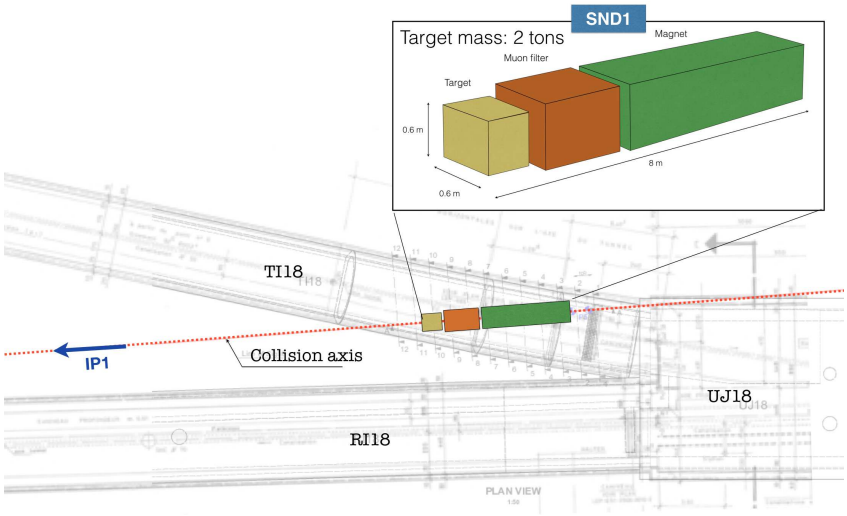

Figure 7. Schematic drawing of an upgraded version of the current detector, beyond Run 3 [2].

The proposed upgrade for each detector in the SND@LHC experiment would consist of three elements. The first element, located upstream, would serve as the target region for vertex reconstruction, and would measure electromagnetic energy, using a calorimetric approach. The second element, positioned downstream, would house the muon identification and hadronic calorimeter system. This system would be followed by a magnet designed for muon charge and momentum measurement. The target region would be constructed using thin, sensitive layers interleaved with tungsten plates, with a total mass of approximately 5 tons. To achieve high-precision vertex reconstruction and electromagnetic energy measurement, compact electronic trackers with a high spatial resolution are being investigated. The use of nuclear emulsion is not feasible, due to technical constraints. The hadronic calorimeter and muon identification system would be optimised, with the goal of exceeding 10 radiation lengths, to enhance muon identification efficiency and improve energy resolution. Additionally, a magnetic field, with a strength of about 1 Tesla, would be applied over a length of approximately 2 m.

The upgraded SND@LHC would provide a unique opportunity to study the physics of heavy flavour production at the LHC, in a region that is not accessible to other experiments.

Author Contributions: These authors contributed equally to this work. All authors have read and agreed to the published version of the manuscript.

Funding: Fundings for the construction and operation of the SND@LHC detector were provided by the following funding agencies: CERN; the Bulgarian Ministry of Education and Science within the National Roadmap for Research Infrastructures 2020–2027 (object CERN); the German Research Foundation (DFG, Deutsche Forschungsgemeinschaft); the Italian National Institute for Nuclear Physics (INFN); JSPS, MEXT, the Global COE program of Nagoya University, the Promotion and Mutual Aid Corporation for Private Schools of Japan for Japan; the National Research Foundation of Korea with grant numbers 2021R1A2C2011003, 2020R1A2C1099546, 2021R1F1A1061717, and 2022R1A2C100505; Fundação para a Ciência e a Tecnologia, FCT (Portugal), CERN/FIS-INS/0028/2021, PRT/BD/153351/2021; the Swiss National Science Foundation (SNSF); TENMAK for Turkey (Grant No. 2022TENMAK (CERN) A5.H3.F2-1). M. Climesu and R. Wanke are funded by the Deutsche Forschungsgemeinschaft (DFG, German Research Foundation), project 496466340. We acknowledge the funding of individuals by Fundação para a Ciência e a Tecnologia, FCT (Portugal) with grant numbers CEECIND/01334/2018, CEECINST/00032/2021 and PRT/BD/153351/2021.

Acknowledgments: We express our gratitude to our colleagues in the CERN accelerator departments for the excellent performance of the LHC. We thank the technical and administrative staffs at CERN and at other SND@LHC institutes for their contributions to the success of the SND@LHC effort.

Conflicts of Interest: The authors declare no conflict of interest.

References

1. Beni, N.; Brucoli, M.; Buontempo, S.; Cafaro, V.; Dallavalle, G.M.; Danzeca, S.; De Lellis, G.; Di Crescenzo, A.; Giordano, V.; Guandalini, C.; et al. Physics Potential of an Experiment using LHC Neutrinos. *J. Phys. G* **2019**, *46*, 115008.
2. Ahdida, C.; De Magistris, M.; Gorshenkov, M.; Zaffaroni, E.; Dedenko, L.; Chernyavskiy, M.; Tioukov, V.; Grenard, J.L.; Vankova-Kirilova, G.; Shirobokov, S.; et al. *SND@LHC—Scattering and Neutrino Detector at the LHC*; Technical report; CERN: Geneva, Switzerland, 2021.
3. Aaij, R.; Beteta, C.A.; Adametz, A.; Adeva, B.; Adinolfi, M.; Adrover, C.; Affolder, A.; Ajaltouni, Z.; Albrecht, J.; Alessio, F.; et al. Measurements of prompt charm production cross-sections in pp collisions at $\sqrt{s} = 13$ TeV. *Nucl. Phys. B* **2016**, *3*, 159. Erratum in: *J. High Energy Phys.* **2016**, *9*, 13. Erratum in: *J. High Energy Phys.* **2017**, *5*, 074. [CrossRef]
4. LHC Collaboration. SND@LHC: The Scattering and Neutrino Detector at the LHC. *arXiv* **2022**, arXiv:2210.02784.
5. Brock, R.; CTEQ Collaboration. Handbook of perturbative QCD: Version 1.0. *Rev. Mod. Phys.* **1995**, *67*, 157. [CrossRef]
6. Conrad, J.M.; Shaevitz, M.H.; Bolton, T. Precision measurements with high-energy neutrino beams. *Rev. Mod. Phys.* **1998**, *70*, 1341.
7. Formaggio, J.A.; Zeller, G.P. From eV to EeV: Neutrino Cross Sections across Energy Scales. *Rev. Mod. Phys.* **2012**, *84*, 1307.
8. De Lellis, G.; Migliozzi, P.; Santorelli, P. Charm physics with neutrinos. *Phys. Rep.* **2004**, *399*, 227. Erratum in: *Phys. Rep.* **2005**, *411*, 323. [CrossRef]
9. Marfatia, D.; McKay, D.W.; Weiler, T.J. New physics with ultra-high-energy neutrinos. *Phys. Lett. B* **2015**, *748*, 113.
10. Argüelles, C.A.; Aurisano, A.J.; Batell, B.; Berger, J.; Bishai, M.; Boschi, T.; Byrnes, N.; Chatterjee, A.; Chodos, A.; Coan, T.; et al. New opportunities at the next-generation neutrino experiments I: BSM neutrino physics and dark matter. *Rep. Prog. Phys.* **2020**, *83*, 124201. [CrossRef]
11. Bustamante, M.; Connolly, A. Extracting the Energy-Dependent Neutrino-Nucleon Cross Section above 10 TeV Using IceCube Showers. *Phys. Rev. Lett.* **2019**, *122*, 041101. [CrossRef]
12. *Scattering and Neutrino Detector at the LHC*; Technical Report CERN-LHCC-2020-013. LHCC-I-037; CERN: Geneva, Switzerland, 2020.
13. Sjöstrand, T.; Mrenna, S.; Skands, P.Z. A Brief Introduction to PYTHIA 8.1. *Comput. Phys. Commun.* **2008**, *178*, 852.
14. Particle Data Group; Zyla, P.; Barnett, R.M.; Beringer, J.; Dahl, O.; Dwyer, D.A.; Groom, D.E.; Lin, C.J.; Lugovsky, K.S.; Pianori, E.; et al. Review of Particle Physics. *Prog. Theor. Exp. Phys.* **2020**, *2020*, 083C01. [CrossRef]
15. Kretzer, S.; Reno, M.H. Tau neutrino deep inelastic charged current interactions. *Phys. Rev. D* **2002**, *66*, 113007. [CrossRef]
16. Roesler, S.; Engel, R.; Ranft, J. The Monte Carlo event generator DPMJET-III. In Proceedings of the Advanced Monte Carlo for Radiation Physics, Particle Transport Simulation and Applications. Proceedings, Conference, MC2000, Lisbon, Portugal, 23–26 October 2000; p. 1033.
17. Fedynitch, A. Cascade Equations and Hadronic Interactions at Very High Energies. Ph.D. Thesis, KIT, Karlsruhe, Germany, 2015. Available online: https://cds.cern.ch/record/2231593 (accessed on 27 November 2015).
18. Böhlen, T.T.; Cerutti, F.; Chin, M.P.W.; Fassò, A.; Ferrari, A.; Ortega, P.G.; Mairani, A.; Sala, P.R.; Smirnov, G.; Vlachoudis, V. The FLUKA Code: Developments and Challenges for High Energy and Medical Applications. *Nucl. Data Sheets* **2014**, *120*, 211. [CrossRef]

19. Hobson, P.R.; Ambrosino, F.; Nozzoli, F.; Cerutti, F.; Ahdida, C.; Bozzato, D.; Calzolari, D.; Cerutti, F.; Charitonidis, N.; Cimmino, A.; et al. New Capabilities of the FLUKA Multi-Purpose Code. *Front. Phys.* **2022**, *9*, 788253. [CrossRef]
20. Agafonova, N.; Alexandrov, A.; Anokhina, A.; Aoki, S.; Ariga, A.; Ariga, T.; Bertolin, A.; Bozza, C.; Brugnera, R.; Buonaura, A.; et al. Final Results of the OPERA Experiment on ν_τ Appearance in the CNGS Neutrino Beam. *Phys. Rev. Lett.* **2018**, *120*, 211801. Erratum in: *Phys. Rev. Lett.* **2018**, *121*, 139901. [CrossRef]
21. Zeus Collaboration. Measurement of high Q^2 charged current cross-sections in e+p deep inelastic scattering at HERA. *Eur. Phys. J. C* **2003**, *32*, 1–16.
22. Sjostrand, T.; Mrenna, S.; Skands, P.Z. PYTHIA 6.4 Physics and Manual. *J. High Energy Phys.* **2006**, *5*, 026.
23. Bellm, J.; Gieseke, S.; Grellscheid, D.; Plätzer, S.; Rauch, M.; Reuschle, C.; Richardson, P.; Schichtel, P.; Seymour, M.H.; Siódmok, A.; et al. Herwig 7.0/Herwig++ 3.0 release note. *Eur. Phys. J. C* **2016**, *76*, 196.
24. Smith, C. On the determination of sin2θw in semileptonic neutrino interactions. *Nucl. Phys. B* **1983**, *228*, 205–215. [CrossRef]
25. Goncharov, M.; Adams, T.; Alton, A.; Bolton, T.; Goldman, J.; Spentzouris, P.; Conrad, J.; Fleming, B.T.; Formaggio, J.; Koutsoliotas, S.; et al. Precise Measurement of Dimuon Production Cross-Sections in ν_μ Fe and $\bar{\nu}_\mu$ Fe Deep Inelastic Scattering at the Tevatron. *Phys. Rev. D* **2001**, *64*, 112006.
26. Kayis-Topaksu, A.Y.S.E.L.; Onengüt, G.; Van Dantzig, R.; De Jong, M.; Oldeman, R.G.C.; Guler, M.; Kose, U.; Tolun, P.; Catanesi, M.G.; Muciaccia, M.T.; et al. Measurement of charm production in neutrino charged-current interactions. *New J. Phys.* **2011**, *13*, 093002.
27. Agafonova, N.; Aleksandrov, A.; Anokhina, A.; Aoki, S.; Ariga, A.; Ariga, T.; Bertolin, A.; Bozza, C.; Brugnera, R.; Buonaura, A.; et al. First observation of a tau neutrino charged current interaction with charm production in the OPERA experiment. *Eur. Phys. J. C* **2020**, *80*, 699.
28. Feng, J.L.; Kling, F.; Reno, M.H.; Rojo, J.; Soldin, D.; Anchordoqui, L.A.; Boyd, J.; Ismail, A.; Harland-Lang, L.; Kelly, K.J.; et al. The Forward Physics Facility at the High-Luminosity LHC. *J. Phys. G* **2023**, *50*, 030501.